Journal of Biomedical Optics

BiomedicalOptics.SPIEDigitalLibrary.org

Fast and improved bioimaging via temporal focusing multiphoton excitation microscopy with binary digital-micromirror-device holography

Yong Da Sie
Chia-Yuan Chang
Chun-Yu Lin
Nan-Shan Chang
Paul J. Campagnola
Shean-Jen Chen

SPIE.

Yong Da Sie, Chia-Yuan Chang, Chun-Yu Lin, Nan-Shan Chang, Paul J. Campagnola, Shean-Jen Chen, "Fast and improved bioimaging via temporal focusing multiphoton excitation microscopy with binary digital-micromirror-device holography," *J. Biomed. Opt.* **23**(11), 116502 (2018), doi: 10.1117/1.JBO.23.11.116502.

Fast and improved bioimaging via temporal focusing multiphoton excitation microscopy with binary digital-micromirror-device holography

Yong Da Sie,[a] Chia-Yuan Chang,[b] Chun-Yu Lin,[b] Nan-Shan Chang,[c,d] Paul J. Campagnola,[e] and Shean-Jen Chen[f,*]
[a]National Cheng Kung University, Department of Engineering Science, Tainan, Taiwan
[b]National Cheng Kung University, Advanced Optoelectronic Technology Center, Tainan, Taiwan
[c]National Cheng Kung University, Institute of Molecular Medicine, Tainan, Taiwan
[d]SUNY Upstate Medical University, Neuroscience and Physiology, Syracuse, New York, United States
[e]University of Wisconsin-Madison, Department of Biomedical Engineering, Madison, Wisconsin, United States
[f]National Chiao Tung University, College of Photonics, Tainan, Taiwan

Abstract. Conventional temporal focusing-based multiphoton excitation microscopy (TFMPEM) can offer widefield optical sectioning with an axial excitation confinement of a few microns. To improve the axial confinement of TFMPEM, a binary computer-generated Fourier hologram (CGFH) via a digital-micromirror-device (DMD) was implemented to intrinsically improve the axial confinement by filling the back-focal aperture of the objective lens. Experimental results show that the excitation focal volume can be condensed and the axial confinement improved about 24% according to the DMD holography. In addition, pseudouniform MPE can be achieved using two complementary CGFHs with rapid pulse-width modulation switching via the DMD. Furthermore, bioimaging of CV-1 in origin with SV40 genes-7 cells demonstrates that the TFMPEM with binary DMD holography can improve image quality by enhancing axial excitation confinement and rejecting out-of-focus excitation. [DOI: 10.1117/1.JBO.23.11.116502]

Keywords: ultrafast lasers; fluorescence microscopy; medical and biological imaging; nonlinear microscopy.

Paper 180379RR received Jun. 28, 2018; accepted for publication Oct. 25, 2018; published online Nov. 15, 2018.

1 Introduction

Temporal focusing (TF)-based multiphoton excitation microscopy (TFMPEM) has been extensively used to offer a broad excitation area with spatial sectioning capability for molecular images and microfabrication.[1–12] The most common TF configuration uses a blazed grating to separate spectral components into monochromatic waves at different spatial angles; then, recombines them at the front-focal plane of an objective lens. Therefore, only in the front-focal plane do the different spectral components overlap in phase and produce a short, high-peak power pulse, allowing MPE to simultaneously occur over the entire projection area. Compared with conventional point-scanning MPE microscopy utilizing spatial focusing to reach a high-photon density in the spot-focal volume,[13] TFMPEM uses spectral dispersion to modulate the optical path of the laser pulse-width to obtain a high-photon density without spatial focusing.[1,2] In this manner, fast- and high-throughput solutions via TF can be achieved. However, widefield TFMPEM has only one line shape at the back-focal plane of the objective; hence, the effective numerical aperture (NA) for focusing efficiency is lessened due to the unfilled back-focal aperture, which means that the axial excitation confinement, at several microns, is inferior to the near one micron by point-scanning MPE. One approach for improving the axial excitation confinement of TFMPEM is to utilize mechanical line-scanning, which involves focusing the laser beam via a cylindrical lens in front of the blazed grating to expand the line-shape beam at the back-focal plane while simultaneously scanning.[14,15] An alternative approach called multifocal TF (MUTF) perpendicularly separates the beam expansion direction into a spectral dispersion via the grating and diffraction of each spectral component with an extra-large-area echelle grating to fill the back-focal aperture of the objective lens without mechanical scanning.[16] Implementing structured light illumination in TFMPEM can also improve the axial resolution based on rejection of the background noise.[17,18]

These three aforementioned methods can improve the axial excitation confinement or axial resolution, and approach the diffraction-limited resolution as intrinsic point-scan MPE microscopy. Nevertheless, the line-scanning scan rate is limited by a one-dimensional (1-D) mechanical scanner at a video rate, while MUTF microcopy requires two grating components to achieve perpendicular spectral dispersion and diffraction for each spectral component in the back-focal plane to improve the axial excitation confinement. In addition, the frame rate of TFMPEM with structured light illumination is decreased due to the need of sequent structured lighting patterns to reconstruct specimen images. Accordingly, improving and optimizing the axial excitation confinement of TFMPEM intrinsically while retaining the advantages of the inherent high-speed widefield imaging and a concise setup would increase the practical application potential for real-time three-dimensional (3-D) molecular image observation. For the purpose of optimizing the back-focal aperture filling without sacrificing the imaging rate with minimal components, the relationship between the blazed grating plane and the back-focal plane of the objective can be

*Address all correspondence to: Shean-Jen Chen, E-mail: sheanjen@nctu.edu.tw

1083-3668/2018/$25.00 © 2018 SPIE

considered as a Fourier transform pair. In this manner, a Fourier hologram can be integrated into the blazed grating plane to offer diffraction light at each spectral component in a direction perpendicular to the spectral dispersion.

To realize the above integration at the blazed grating plane, a digital-micromirror-device (DMD) is incorporated into the optical setup. In our previous study,[19,20] a DMD was used to not only replace the blazed grating as the spectral dispersion for TF but also generate arbitrary patterns. In this study, the optimized diffraction light to fill the back-focal aperture was calculated first as a binary computer-generated Fourier hologram (CGFH),[21–23] and with two complementary CGFHs at rapid pulse width modulation (PWM) switching, a pseudouniform TF-excitation plane can be achieved by the DMD. Currently, the back-focal aperture size of the objective lens is about 9 mm and so the size of the line-shape beam at the back-focal plane in the current setup also approaches 9-mm long; therefore, the purpose of the designed CGFH is to expand the line-shape spectral components to fully fill the back-focal aperture. The additional benefit of this scheme is that it can be adapted to different TFMPEM systems by simply redesigning the binary CGFH. More specifically, the DMD pattern would not add additional spectral dispersion,[19] and the binary CGFH only influences the diffraction of each spectral component independently to compress the TF excitation volume in the axial direction for improving the sectioning capability intrinsically while rejecting some of the back-ground signals and out-of-focus signals. Finally, the two-photon excitation fluorescent (TPEF) image of CV-1 in origin with SV40 genes-7 (COS-7) cell is demonstrated that the TFMPEM with binary DMD holography can improve image quality by way of the axial excitation confinement.

2 Principle and Optical Setup

2.1 *Axial Excitation Confinement*

The axial image resolution of TFMPEM is based on two major parts such as the axial excitation confinement, which is related to the excitation wavelength and spectral components of the light source, the dispersion distortion of the spectral components in the optical path, the NA of the objective, and the back-focal plane filling; and, the emission collection capability, which is related to the emission wavelength of the sample and the NA of the objective. Herein, the axial excitation confinement is considered; hence, the axial excitation profile is described. First, the Rayleigh range z_R is defined as[15]

$$Z_R = \frac{f^2\lambda}{\pi D^2}, \tag{1}$$

where λ is the excitation wavelength, f is the focal length of the objective, and D is the full aperture size. Through Eq. (1), the beam axial excitation normalized profile can be inferred, as shown in Fig. 1. Herein, Δz is the axial distance relative to the axial position of the front-focal plane. Figure 1 shows a comparison of the axial excitation profile, the beam shape at the back-focal plane, and the excitation pattern at the front-focal plane among five different MPE microscopes based on conventional point scanning, line scanning, TF, line-scanning TF, and MUTF mechanisms with intrinsic optical sectioning.[14–16] The conventional point scanning and line scanning are based on two- and one-directional spatial focusing, respectively. The beam shape and excitation patterns at the back-focal and front-focal planes can respectively elucidate the beam lateral profile at the Fourier and conjugate Fourier planes. The TF, line scanning TF, and MUTF are all based on TF-excitation via a blazed grating to enable spectral dispersion. Further, the line scanning TF combines spatial focusing via a cylindrical lens to fill the back-focal aperture of the objective. In the same way that the line scanning TF fills the back-focal aperture, the MUTF uses an extra echelle grating to diffract each spectral component. Two kinds of beam axial-excitation profiles are shown in Fig. 1, the only difference being the beam shape at the back-focal plane of the objective, namely full filling or just a line at the back-focal aperture of the objective. Accordingly, the profile can be summarized as the comparison between the fully filled and line-shape filled aperture at the back-focal plane, with the difference being in the power coefficient, i.e., -1 or $-1/2$.

The axial excitation confinement will affect the axial image resolution by reducing the background signal excitation. From the illustration in Fig. 1, the improvement in the optical sectioning ability of our developed TFMPEM with DMD is concentrated to further confine the axial excitation volume via fully filling the back-focal aperture of the objective using binary CGFH. In this manner, it is possible to improve the axial excitation confinement of TF to approach those of line scanning and MUTF while retaining the fast and concise widefield excitation of the developed TFMPEM without a mechanical line scanner and a large-area echelle grating.

	Conventional point scanning	Conventional line scanning	Temporal focusing (TF)	Line scanning TF [15]	MUTF [16] & Method in this paper
Beam axial excitation profile	$\sim\left[1+\left(\frac{\Delta z}{z_R}\right)^2\right]^{-1}$	$\sim\left[1+\left(\frac{\Delta z}{z_R}\right)^2\right]^{-\frac{1}{2}}$	$\sim\left[1+\left(\frac{\Delta z}{z_R}\right)^2\right]^{-\frac{1}{2}}$	$\sim\left[1+\left(\frac{\Delta z}{z_R}\right)^2\right]^{-1}$	$\sim\left[1+\left(\frac{\Delta z}{z_R}\right)^2\right]^{-1}$
Beam shape at back-focal plane					
Excitation pattern at front-focal plane					

Fig. 1 Comparison of axial excitation profiles, beam shapes at the back-focal plane, and excitation patterns at the front-focal plane among five different multiphoton excitation systems.

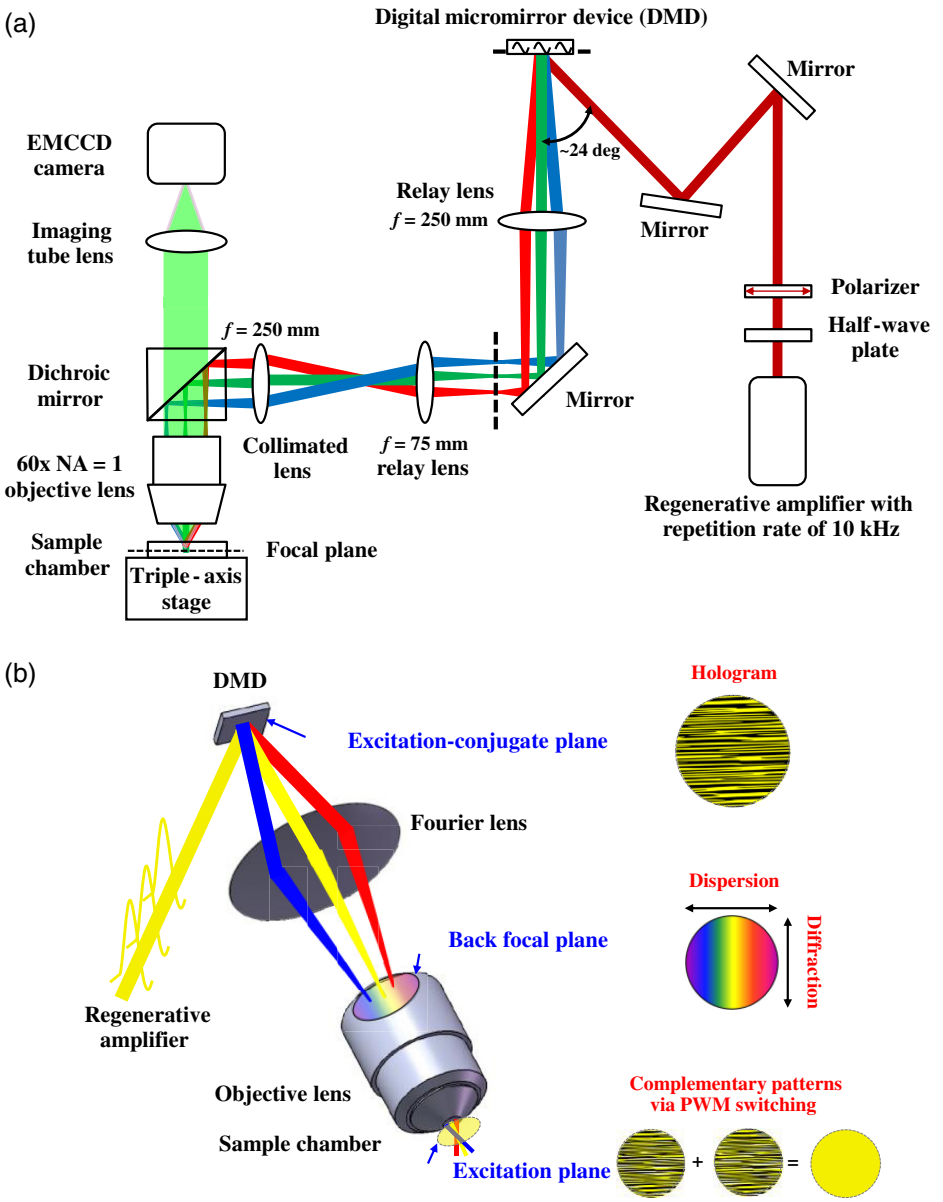

Fig. 2 (a) Optical setup of TFMPEM with the DMD as the grating dispersion and spatial modulation, which is similar to our previous research.[19] (b) A new progress here includes binary CGFH on the excitation-conjugate plane via the DMD, the spectral dispersion for the TF effect and the diffraction for filling the back-focal aperture, and the two complementary excitation patterns on the MPE plane via rapid PWM switching.

2.2 *Temporal Focusing Multiphoton Excitation Microscope with Digital-Micromirror-Device*

Figure 2(a) shows a schematic diagram of the developed TFMPEM with computer-controlled DMD. The overall setup includes a Ti:sapphire ultrafast regenerative amplifier (Spitfire Pro, Spectra-Physics) coupled with a Ti:sapphire ultrafast oscillator (Tsunami, Spectra-Physics) as the seed beam of the amplifier, an upright optical microscope (Axio imager.A2m, Carl Zeiss, Germany), a triple-axis sample positioning stage (H101A ProScan, Prior Scientific, UK), a piezo stage (NanoScanZ 200, Prior Scientific, UK), an EMCCD camera (iXon Ultra 897, Andor, UK) with a camera adapter (T2-T2 SLR 2.5X, Carl Zeiss, Germany) to magnify the images 2.5X, a data acquisition card with a field-programmable gate array module (PCIe-7842R, National Instruments), and a DMD with 0.7-in. diagonal micromirror array with 12-deg tilt-angle micromirrors on the chip (DLP7000, Texas Instrument). The amplifier has a pulse energy of 400 μJ/pulse, a pulse width of 100 fs, and a repetition rate of 10 kHz, which is sufficient for TPEF of an ~200- × 200-μm^2 area, while a blazed grating functions as the dispersion device.[9] However, the current excitation area is around 40×40 μm^2 due to the restrictions by the 0.7–in. size and the 12-deg tilt angle of the DMD. The DMD replaces the blazed grating as the spectral dispersion for TF; therefore, according to the diffraction equation, the incidence angle should be close to twice the tilt angle of 12 deg to reach the maximum diffraction efficiency.[19] Herein, the incident angle is adjusted to 24.4 deg as the diffraction order of 10, the central wavelength of 800 nm of the ultrafast amplifier, and the effective pitch of the micromirrors is 19.35 μm, due to the flip axis being on the

diagonal direction of each micromirror. Furthermore, a half-wave plate and a linear polarizer first adjust power and maintain the horizontal polarization of the beam from the amplifier while a mechanical shutter controls the excitation time to prevent unnecessary exposure. A set of relay lenses with focal lengths of 200 and 80 mm was inserted to lengthen the beam path and adjust the beam size to fit the back-focal aperture of the objective lens as a Fourier lens. The dispersed beam propagates through the $4f$ setup, which comprises a collimating lens and a 60× objective lens with a NA 1.2 (UPlanSApo 60XW/NA 1.2, Olympus, Japan).

The binary CGFH pattern at the top-right of Fig. 2(b) can be implemented via the DMD placed at the excitation-conjugate plane; meanwhile, the Fourier transform of the CGFH is converted via the Fourier lens onto the back-focal plane. Therefore, the beam shape of each spectral component at the back-focal plane could be implemented using binary CGFH via the DMD. Accordingly, the DMD not only implements spectral dispersion for different spectral components as with a blazed grating but also produces diffraction light at each spectral component perpendicular to the spectral dispersion via a designed CGFH. The TFMPEM setup enables each spectral component to be independently diffracted via the DMD with a designed CGFH, after which the Fourier transform of the CGFH can be projected onto the Fourier plane (i.e., ack-focal plane) through the Fourier lens, as shown at the mid-right of Fig. 2(b). Finally, the objective performs the beam-shape Fourier transform of each spectral component, and then recombines them at the front-focal plane. As such, only in the front-focal plane do the different spectral components overlap in phase and produce a short, high-peak power pulse with the conjugated CGFH pattern, as shown at the bottom-right of Fig. 2(b). Although this allows MPE to simultaneously occur over the entire projection area, the patterned illumination of CGFH cannot offer a uniform excitation plane for matching the image quality requirement. The bottom-right of Fig. 2(b) also presents the concept of using the rapid DMD's PWM switching to produce a pseudo-uniform excitation pattern by combining two complementary binary CGFH patterns.

2.3 *Binary Computer-Generated Fourier Hologram*

As shown in Fig. 2, the CGFH is governed by the Fresnel diffraction with a Fourier lens (i.e., raunhofer diffraction with the Fourier transform relation between the hologram and the reconstructed image) to perform the Fourier transform. An original intensity CGFH can be acquired by first executing the inverse Fourier transform of the designed beam shape, which is a line perpendicular to the spectral dispersion, and then simply weighting the intensity information of the inverse Fourier transform by the intensity distribution of the laser source beam. The phase information is neglected. The DMD can only produce instant binary intensity, so the original intensity CGFH must be converted to a binary CGFH. Herein, the binary Gerchburg–Saxton (GS) algorithm[21] is chosen to calculate the binary CGFH, the advantages of which are good diffraction efficiency, simple and fast evaluation of a binary CGFH with fast Fourier transform iteration to optimize the hologram, and high convergence speed.[21,23] Currently, the back focal aperture of the 60× objective lens is about 9 mm in diameter; therefore, the DMD should diffract the regenerative amplifier's output with a 10-mm beam size to completely fill the objective lens' aperture at the Fourier plane according to an excitation wavelength of around 800 nm, a DMD pixel size of around 13.6 μm, and the 250-mm focal length of the Fourier lens.

2.4 *Theoretical Analysis of Temporal Focusing-Based Multiphoton Excitation Microscopy*

To explicate our experimental results, theoretical analysis based on Fourier optics is adopted to evaluate the axial confinement of our TFMPEM system. As we know that an ultrashort pulse is generated by superposition of light with different wavelengths in phase. Hence, an ultrashort pulse passes through a grating in the TFMPEM can be decomposition of plane waves of different wavelengths in a different diffractive angle θ_ω that can calculate from the grating equation. After passing through the collimated lens, decomposed plane wave of different wavelengths is focused on the back aperture plane of an objective in different focal points. Then, electric field distribution with a different wavelength A_F is filter by the back aperture (circular aperture) of an objective. After that, the Fourier transform in a space domain based on the theory of Fourier optics is adopted to calculate the electric field distribution of different wavelengths in the TF plane (imaging plane) A_{TF}

$$\sum A_{TF}(x,y;\omega) = \sum FT_{\text{space}}\left\{A_F(u - f\cdot\tan\theta_\omega, v;\omega) \cdot \text{circ}\left(\frac{\sqrt{u^2+v^2}}{R_0}\right)\right\}, \tag{2}$$

where A is an electric field distribution, ω is the angular frequency of light, θ is the diffractive angle, f is the focal length of collimated lens, R_0 is the radius of back aperture for an objective, and the subscripts F and TF denote the back-aperture plane and TF plane. FT_{space} represents the Fourier transform in a space domain. It is important that electric field distribution A_F is the Fourier transform in space domain for the pattern of Holo-1 and Holo-2 on DMD in this theoretical simulation. Finally, a time-domain electric field profile of an ultrashort pulse in the TF plane is obtained from the electric field distribution A_{TF} using the Fourier transform in a time domain:

$$I_{TF}(x,y;t) = \left|FT_{\text{time}}\{\sum A_{TF}(x,y;\omega)\}\right|^2, \tag{3}$$

for a two-photon excitation, time-varying fluorescence signal I_{2P} is linear to the square of intensity profile I_{TF} of an ultrashort pulse in the TF plane. FT_{time} denotes the Fourier transform in a time domain. Overall time-average fluorescence signal in the TF plane is a time- and space-domain integration of the fluorescence signal I_{2P}. To obtain the time-varying fluorescence signal in the defocus plane of the TFMPEM, the Helmholtz equation is adopted to calculate an electric field distribution in the defocus plane. According to the Helmholtz equation, an electric field distribution in the defocus plane Δz is simply a change in the relative phases of an electric field distribution in the TF plane.[24] This means the probability of a two-photon excitation varies along the axial direction, and the cutoff frequency will also decrease along the defocus or out-of-focus direction. The electric field at the point near the focus in terms of the projected sectorial pupil is multiplied by a defocus term.

3 Experimental Results and Discussions

3.1 *Axial Confinement Enhancement via Binary Digital-Micromirror-Device Holography*

A PMMA thin film doped with rhodamine-6G (R6G) dye (<200-nm thick) and prepared via spin coating[18] was first placed on the front-focal plane of the objective lens for TPEF imaging. Figures 3(a) and 3(b) show images of the beam shape near the back-focal aperture of the objective lens and the TPEF images at the front-focal plane, respectively. The images from left to right are: TF spectral dispersion only (without the CGFH diffraction), TF spectral dispersion with 0.58-μm^{-1} spatial-frequency sinusoidal structured diffraction, TF spectral dispersion with CGFH diffraction at the optimized expansion (almost filling the aperture), and TF spectral dispersion with CGFH diffraction at an expansion exceeding the aperture (twofold expansion greater than the aperture). Figure 3(c) shows the normalized intensities of the red-dashed lines in Fig. 3(a). From the results, it can be seen that utilizing the binary CGFH can precisely and efficiently control the diffraction light at each spectral component on the back-focal plane and optimize it according to the back-focal aperture size to exploit the full NA of the excitation light. The $\pm$1st order diffraction intensity at the optimized CGFH diffraction condition (named Holo-1) has more condensed diffraction light than those at the non-optimized conditions (termed Holo-2), and therefore produces superior axial confinement. The TF spectral-dispersion result with the 0.58 μm^{-1} sinusoidal structured diffraction (denoted as Sinusoidal) shows that the energy can be specifically diffracted to partially fill the aperture; hence, the axial excitation confinement can be improved.

The prepared fluorescent PMMA thin film was examined to verify and demonstrate the axial confinement improvement via the four different TF excitation conditions (TF, Sinusoidal, Holo-1, and Holo-2) as shown in the simulation of Fig. 4. From the simulation comparison of Fig. 4, Holo-1 and Holo-2 can fill-in more of the back focal aperture; therefore, the ACE of Holo-1 and Holo-2 are superior to that of TF. The film was axially scanned with a range of 20 μm and a step size of 0.5 μm by controlling the piezomotorized stage. Figure 4 shows the axial MPE fluorescent intensity profiles of the PMMA thin

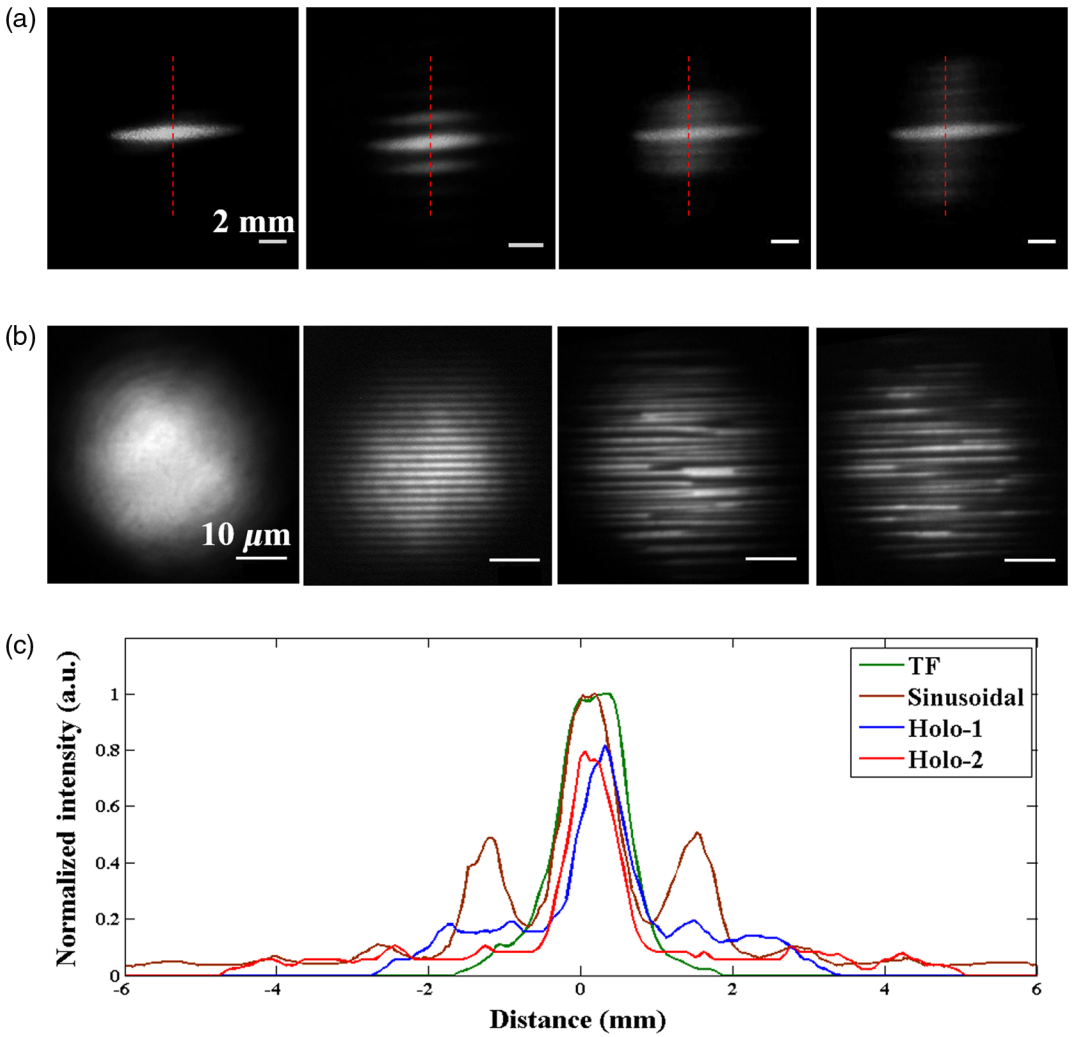

Fig. 3 (a) Beam shape images close to the back-focal aperture (from left to right) by TF spectral dispersion only (TF); TF spectral dispersion with sinusoidal structured diffraction (Sinusoidal); TF spectral dispersion with optimized CGFH diffraction (Holo-1); and, TF spectral dispersion with CGFH diffraction (Holo-2) at the twofold expansion over the aperture. The spectral dispersion direction here is horizontal. (b) TPEF images at the four different TF excitation conditions in (a). (c) Normalized intensity profiles of red-dashed lines cut from (a).

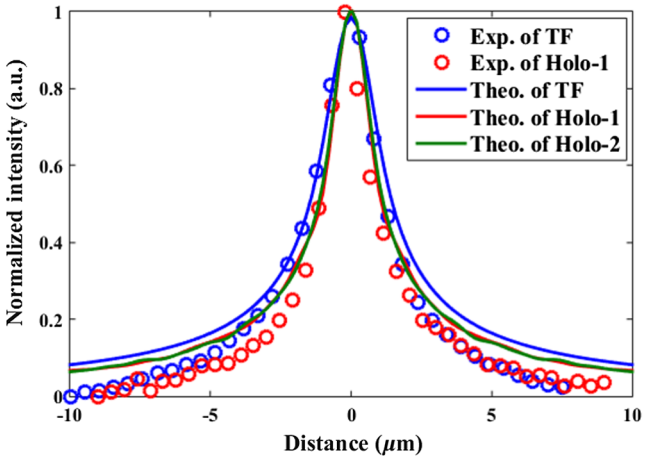

Fig. 4 Axial MPE fluorescence intensity profiles of the thin film under TF (blue circle) and Holo-1 (red circle). Theoretical analysis of axial MPE fluorescence intensity profiles for TF (blue line), Holo-1 (red line), and Holo-2 (green line).

film under the aforementioned four conditions. In the experimental results of Fig. 4, the excitation energy and the exposure time of each curve are the same and normalized with the maximum intensity of each curve, and then fitted with a spatially-chirped beam fitting equation to determine the full width at half maximum (FWHM).[25] The axial excitation depths fitted with spatially-chirped beam fitting equation [26] are around 2.94 and 2.37 μm (FWHM) for the TF and Holo-1 conditions, respectively. Theoretical analysis of axial MPE fluorescence intensity profiles for TF (blue line) and Holo-1 (red line). The simulated axial resolutions of TF and Holo-1 are around 2.93 and 2.35 μm, respectively. In comparison, the axial excitation depth with the Holo-1 condition was improved to nearly 2.37 μm [about $(2.94 - 2.37)/2.37 \times 100\% = 24\%$]. Moreover, it can be seen from the results of Fig. 4 that not only does the FWHM of the optimized CGFH decrease by fully filling the back aperture of the objective lens, but the excitation intensity is also reduced in both sides of spatially chirped beam fitting profile. Accordingly, to further improve axial excitation confinement in the TFMPEM, two modifications can be considered. One is to use similar sinusoidal frequency combinations to design the periodic illumination pattern; however, this approach requires providing a uniform excitation pattern despite the rapid PWM switching. The other remains adopting CGFH diffraction; but to increase diffraction efficiency, the binary intensity DMD can be replaced with a gray-level phase generator, such as a spatial light modulator.[25–27] Nevertheless, a blazed grating or a DMD is still required for spectral dispersion in the DMD-based TFMPEM setup.

Repeat the above process of calculation of Sec. 2.4 that overall time-average fluorescence signal in the defocus plane can be obtained. According to these theoretical analyses, an axial resolution of the TFMPEM with different pattern on DMD can be

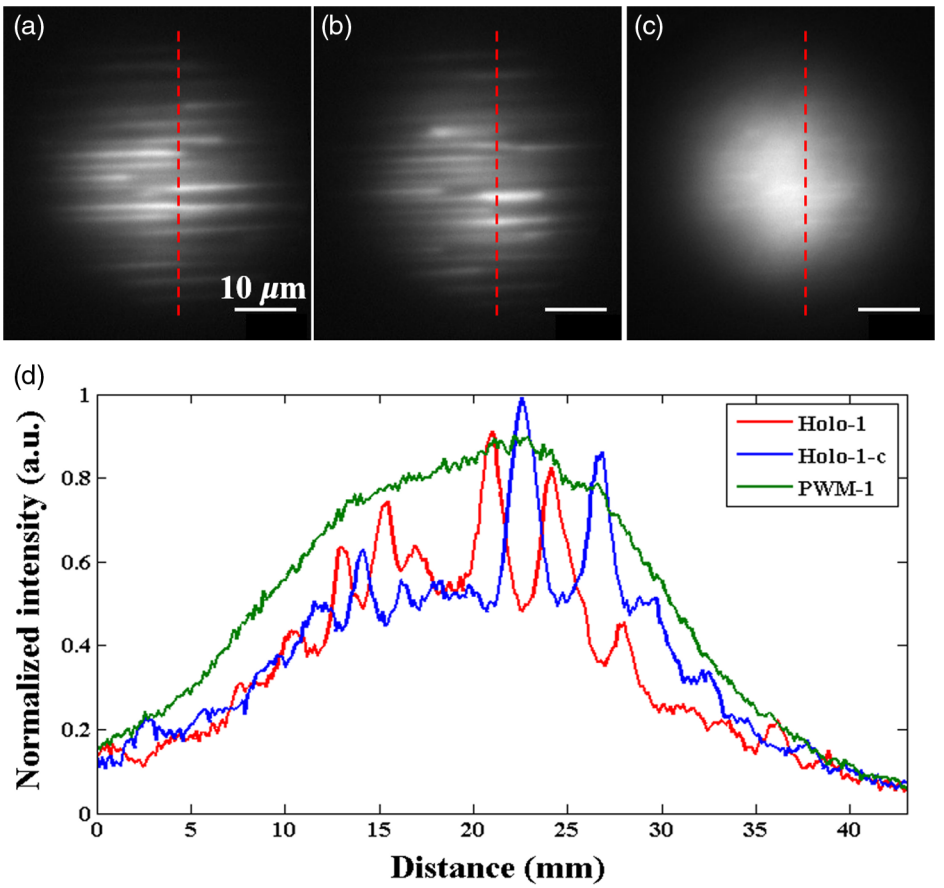

Fig. 5 (a) & (b) TPEF images by TF with the original and complementary CGFH excitation patterns via rapid PWM switching, respectively. The intensity of each pattern is nearly the inverse of the other. (c) Merged image showing near-uniform excitation. (d) Cross-section profiles of the red-dashed lines from (a) to (c).

evaluation. The theoretical analysis is shown in Fig. 4. It is clear to see that the axial resolution is an enhancement by the binary DMD holography. In our simulated results, axial resolution that is also fitted with spatially chirped beam fitting equation is around 2.93 and 2.35 μm for the TF and Holo-1 conditions, respectively. Axial resolution in our simulated results is similar to our experimental results and demonstrates that the TFMPEM with binary DMD holography can improve image quality through enhancing axial excitation confinement and rejecting out-of-focus excitation.

3.2 *Complementary Patterned Illumination via Pulse Width Modulation*

From the results in Fig. 3, it is illustrated that via the optimized binary CGFH, each spectral component of the ultrafast laser beam can be expanded to a vertical line-like shape on the back focal plane; meanwhile, the different spectral components are dispersed to a horizontal line shape via the DMD spectral dispersion. The average excited power on the sample was controlled to below 20 mW with an exposure time of 100 ms. Accordingly, the different spectral components can be horizontally dispersed and vertically diffracted to fully fill the back-focal aperture. However, in the multiphoton excitation plane, the excitation pattern is binary-interference shaped due to the initial phase of our chosen light source being in random phase distribution; therefore, uniform excitation is not possible. To overcome this problem, the PWM is taken into consideration with respect to the characteristics of the DMD.[28] Because the light intensity control of the DMD is operated with fast-flips of each micromirror, the time of each mirror is governed/controlled by the 8-bit coding with gray-levels of 0 to 255. Due to the display of the DMD projector being based on persistence of vision, the different gray-levels represent the different remaining action times of each micromirror. For 8-bit coding, the gray-levels of 127 and 128 have similar remaining action times. Therefore, to demonstrate the concept of binary CGFH for TFMPEM, two complementary excitation patterns, both of which contain the effect of the Fourier hologram, with respective gray-levels of 127 and 128 via the PWM are sequentially switched to produce a pseudouniform excitation, as shown at the bottom-right of Fig. 2. Figures 5(a) and 5(b), respectively, show the original and complementary CGFH excitation patterns via rapid PWM switching, the pattern intensities of which are nearly the inverse of each other. Figure 5(c) is the merged excitation pattern and features near-uniform excitation. Furthermore, Fig. 5(d) presents the cross-section profiles of the red-dashed lines from Figs. 5(a)–5(c). As seen in Fig. 5(d), the numerous peaks and valleys of Holo-1 and Holo-1-c are nearly complementary. Comparatively, the PWM-1 curve reveals a smoother Gaussian distribution.

3.3 *Bioimaging for COS-7 Cell*

To demonstrate the axial confinement improvement in practical application, the COS-7 cell line was stained with secondary antibody Alexa Fluor 488 fluorescein, after which the cytoskeleton's α-tubulin was imaged by TF alone [Fig. 6(a)] and TF with the two complementary CGFH excitation and mergence approach [Fig. 6(b)]. Furthermore, to avoid photobleaching, the average excited power on the sample was controlled to below 20 mW with an exposure time of 200 ms. The filtered images, after the iterative deconvolution process, are respectively

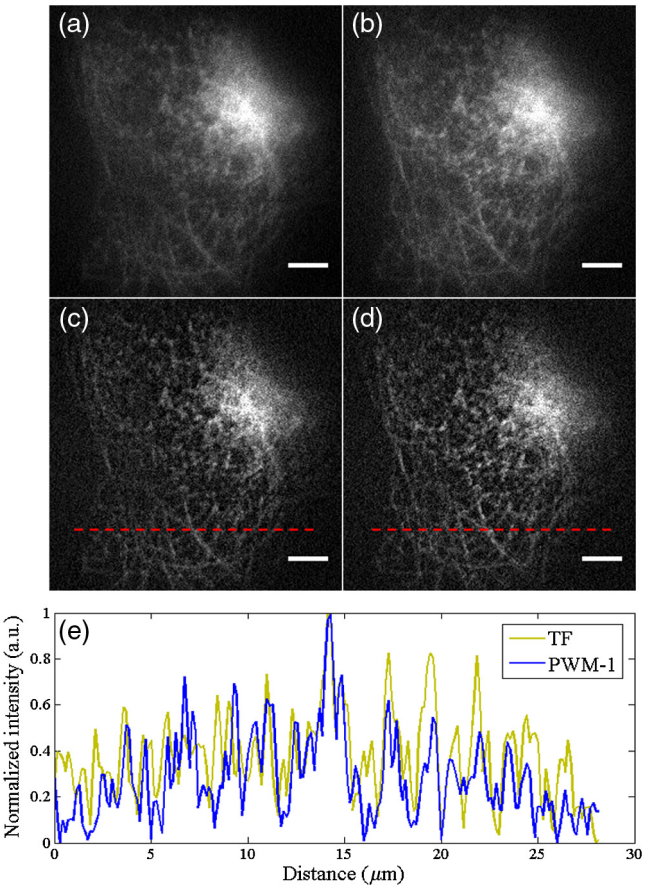

Fig. 6 TPEF images of α-tubulin of the COS-7 cell line stained with Alexa Fluor 488 by (a) TF only, and (b) TF with the two complementary CGFH excitation. (c) and (d) Filtered images of (a) and (b) after iterative deconvolution process. (e) Intensity profiles along the intersecting red dashed lines in Figs. 6(c) and 6(d). Scale bar: 5 μm.

shown in Figs. 6(c) and 6(d). In comparing Figs. 6(a) and 6(b), it can be seen that a sharper image via the TF with the complementary CGFH approach can be obtained through enhancing axial excitation confinement. This TF method with DMD-based CGFH diffraction targets axial excitation confinement improvement; consequently, a portion of the background noise in TFMPEM is rejected. Therefore, the image contrasts of Figs. 6(b) and 6(d), respectively, compared with those of Figs. 6(a) and 6(c) are superior. From the TPEF images of Figs. 6(b) and 6(d), and with the support of rapid PWM switching, a near-uniform TPEF image can be achieved even with the binary CGFH pattern excitation. Figure 6(e) shows the section profiles of the red-dashed lines in Figs. 6(c) and 6(d). Due to the ACE becoming narrower, some details in Fig. 6(b) can be slightly clarified via this approach. The overall improvement, however, is minor due to the low power efficiency.

4 Conclusions

The successful simultaneous spectral dispersion and diffraction of two-dimensional light expansion on the back-focal aperture via only one DMD with optimized CGFH was demonstrated to provide around 24% of improvement in the excitation volume plane. This study was based on our TF system with DMD-based spectral dispersion,[19] the GS-based binary CGFH via the same DMD, and rapid PWM switching for pseudouniform excitation. On the basis of these TF ideas, binary CGFH optimization was

calculated and used to fill the back-focal aperture of the objective. However, the DMD diffraction efficiency of binary intensity holography is relatively low and the power loss exceeds 50%. In addition to an increase in the laser power, a phase generator, such as a spatial light modulator, can be utilized to provide phase holography with superior diffraction efficiency. Moreover, the improvement to the excitation volume and axial-sectioning can also intrinsically extend the scope and potential of fast and real time 3-D molecular imaging by decreasing the out-of-focus excitation energy and filling the excitation NA. Bioimaging of COS-7 cells demonstrates that the TFMPEM with binary DMD holography can improve image quality through enhancing axial excitation confinement and rejecting out-of-focus excitation.

Disclosures

The authors have no relevant financial interests in this article and no potential conflicts of interest to disclose.

Acknowledgments

This study was financially supported by the Ministry of Science and Technology (MOST) of Taiwan (MOST 104-2221-E-006-172-MY3, MOST 104-2221-E-006-064-MY3).

References

1. D. Oron, E. Tal, and Y. Silberberg, "Scanningless depth-resolved microscopy," *Opt. Express* **13**(5), 1468–1476 (2005).
2. G. Zhu et al., "Simultaneous spatial and temporal focusing of femtosecond pulses," *Opt. Express* **13**(6), 2153–2159 (2005).
3. A. Vaziri et al., "Multilayer three-dimensional super resolution imaging of thick biological samples," *Proc. Natl. Acad. Sci. U. S. A.* **105**(51), 20221–20226 (2008).
4. E. Papagiakoumou et al., "Scanless two-photon excitation of channelrhodopsin-2," *Nat. Methods* **7**(10), 848–854 (2010).
5. D. Kim and P. T. C. So, "High-throughput three-dimensional lithographic microfabrication," *Opt. Lett.* **35**(10), 1602–1604 (2010).
6. D. N. Vitek et al., "Temporally focused femtosecond laser pulses for low numerical aperture micromachining through optically transparent materials," *Opt. Express* **18**(17), 18086–18094 (2010).
7. D. Therrien et al., "Wide-field multiphoton imaging of cellular dynamics in thick tissue by temporal focusing and patterned illumination," *Biomed. Opt. Express* **2**(3), 696–704 (2011).
8. J.-Y. Yu et al., "Wide-field optical sectioning for live-tissue imaging by plane-projection multiphoton microscopy," *J. Biomed. Opt.* **16**, 116009 (2011).
9. L.-C. Cheng et al., "Spatiotemporal focusing-based widefield multiphoton microscopy for fast optical sectioning," *Opt. Express* **20**(8), 8939–8948 (2012).
10. Y.-C. Li et al., "Fast multiphoton microfabrication of freeform polymer microstructures by spatiotemporal focusing and patterned excitation," *Opt. Express* **20**(17), 19030–19038 (2012).
11. H. Dana and S. Shoham, "Remotely scanned multiphoton temporal focusing by axial grism scanning," *Opt. Lett.* **37**(14), 2913–2915 (2012).
12. C. G. Durfee and J. A. Squier, "Breakthroughs in photonics 2014: spatiotemporal focusing: advances and applications," *IEEE Photonics J.* **7**(3), 1–6 (2015).
13. P. T. C. So, E. Y. S. Yew, and C. Rowlands, "High-throughput nonlinear optical microscopy," *Biophys. J.* **105**(12), 2641–2654 (2013).
14. E. Tal, D. Oron, and Y. Silberberg, "Improved depth resolution in video-rate line-scanning multiphoton microscopy using temporal focusing," *Opt. Lett.* **30**(13), 1686–1688 (2005).
15. M. E. Durst, G. Zhu, and C. Xu, "Simultaneous spatial and temporal focusing in nonlinear microscope," *Opt. Commun.* **281**(7), 1796–1805 (2008).
16. A. Vaziri and C. V. Shank, "Ultrafast widefield optical sectioning microscopy by multifocal temporal focusing," *Opt. Express* **18**(19), 19645–19655 (2010).
17. H. Choi et al., "Improvement of axial resolution and contrast in temporally focused widefield two-photon microscopy with structured light illumination," *Biomed. Opt. Express* **4**(7), 995–1005 (2013).
18. L.-C. Cheng et al., "Nonlinear structured-illumination enhanced temporal focusing multiphoton excitation microscopy with a digital micromirror device," *Biomed. Opt. Express* **5**(8), 2526–2536 (2014).
19. J.-N. Yih et al., "Temporal focusing-based multiphoton excitation microscopy via digital micromirror device," *Opt. Lett.* **39**(11), 3134–3137 (2014).
20. C.-Y. Chang et al., "Temporal focusing-based widefield multiphoton microscopy with spatially modulated illumination for biotissue imaging," *J. Biophotonics* **11**(1), e201600287 (2018).
21. R. W. Gerchberg and W. O. Saxton, "A practical algorithm for the determination of phase from image and diffraction plane pictures," *Optik* **35**(2), 237–246 (1972).
22. J. Cheng et al., "High-speed femtosecond laser beam shaping based on binary holography using a digital micromirror device," *Opt. Lett.* **40**(21), 4875–4878 (2015).
23. J. Cheng et al., "Ultrafast axial scanning for two-photon microscopy via a digital micromirror device and binary holography," *Opt. Lett.* **41**(7), 1451–1454 (2016).
24. J. W. Goodman, *Introduction to Fourier Optics*, McGraw-Hill, New York (1996).
25. S.-Y. Wu, J. Liang, and M. F. Becker, "Suppression of the zero-order diffraction beam from computer-generated holograms produced by a DLP® spatial light modulator," *Proc. SPIE* **8254**, 82540C (2012).
26. M. E. Durst, G. Zhu, and C. Xu, "Simultaneous spatial and temporal focusing for axial scanning," *Opt. Express* **14**(25), 12243–12254 (2006).
27. E. Papagiakoumou et al., "Temporal focusing with spatially modulated excitation," *Opt. Express* **17**(7), 5391–5401 (2009).
28. D. Dudley, W. Duncan, and J. Slaughter, "Emerging digital micromirror device (DMD) applications," *Proc. SPIE* **4985**, 14–25 (2003).

Yong Da Sie received his PhD from the Department of Engineering Science of National Cheng Kung University (NCKU), Taiwan, in 2018. Main research subjects are focusing on multiphoton microfabrication of bio-scaffold, and temporal focusing-based light-field microscopy.

Chia-Yuan Chang is an assistant research fellow at Advanced Optoelectronic Technology Center (AOTC), NCKU, Taiwan. His research focuses on multiphoton microscopy, temporal focusing-based multiphoton microscopy, and fast adaptive optics system integration for the potential for deep tissue imaging. He obtained his PhD from the Department of Photonics of NCKU, Taiwan.

Chun-Yu Lin is an assistant research fellow at AOTC, NCKU, Taiwan. His research focuses on multiphoton-excited fluorescence, plasmon-enhanced two-photon excited fluorescence, and multiphoton-induced 3D fabrication techniques. He obtained his PhD of Department of Engineering Science from NCKU, Taiwan.

Nan-Shan Chang is currently a professor at the Molecular Medicine Institute, NCKU in Taiwan, and an adjunct professor with the SUNY Upstate Medical University and the NYS Institute for Basic Research in Developmental Disabilities, New York. He is most noted for his discovery of tumor suppressor WWOX in 2000.

Paul J. Campagnola is a professor in the departments of biomedical engineering and physics at the University of Wisconsin—Madison. His research focuses on the development of nonlinear optical spectroscopy and microscopy methods, with an emphasis on translational applications. These research efforts are directed at understanding cancer cell–ECM interactions in the tumor microenvironment as well as fabricating scaffolds for tissue regeneration.

Shean-Jen Chen received his PhD for research in adaptive noise cancellation and image restoration at University of California, Los Angeles (UCLA) in 1996. Currently, he is a professor and the dean in the College of Photonics, National Chiao Tung University, Taiwan. He is actively engaged in researching advanced nonlinear optical microscopy and three-dimensional photolithography.